Tellus (1997), 49B, 199–215
Printed in UK – all rights reserved



TELLUS
ISSN 0280–6509

# Dependence of trajectory accuracy on the spatial and temporal densities of wind data

By TAE-YOUNG LEE*, SANG-WOOK PARK and SEUNG-BUM KIM, *Department of Astronomy and Atmospheric Sciences, Yonsei University, Seodaemoon-Ku, Seoul 120–749, Korea*

(Manuscript received 19 March 1996; in final form 1 November 1996)

ABSTRACT

An investigation has been carried out to evaluate the dependence of trajectory accuracy on the density of wind data. The present study has applied an observing system simulation technique to 3 meteorological episodes over eastern Asia. A mesoscale numerical model with a horizontal grid size of 20 km has been employed to generate the reference atmospheric fields. Particles are initially located at 3 isobaric levels (925, 850 and 700 hPa). The results indicate that the 3-dimensional trajectories are sensitive to both the temporal and spatial densities of wind data. The trajectories show relatively strong sensitivity to the temporal density change between 6- and 12-h intervals in general, and also to the spatial density change between 160- and 320-km intervals in one of the cases. The effectiveness of enhancing either the temporal or spatial resolution of wind data for the improvement of trajectory accuracy is found to vary with the meteorological situation. When the intervals of 12 h and 320 km are assumed to be the resolution of wind observations, enhancing the spatial resolution to 160-km interval improves the accuracy more than enhancing the temporal resolution to 6-h intervals in a case with an excursion of the Siberian High. However the opposite is true in the other 2 cases in which either a synoptic scale cyclone or a low pressure system with significant diabatic heating is important, although the difference in the accuracy improvements is small in 1 of the 2 cases. It is also found that the estimated accuracy of a trajectory model and its sensitivity to wind data density may vary significantly with the resolution of the reference wind data sets: the use of reference wind data with low resolution can result in a significant underestimation of transport error and may exaggerate the effectiveness of enhancing the temporal resolution for the improvement of trajectory accuracy. The accuracy of an isobaric model is generally comparable to that of a 3-dimensional model, when data sets with 12-h, 320-km resolution are used. Under a strongly baroclinic condition, however, the isobaric model can give a very large trajectory error.

## 1. Introduction

Trajectory calculations are frequently used to find the source-receptor relationship for air pollution problems associated with long-range transport. Their accuracies have been a subject of considerable interest. Trajectory accuracy is limited by the spatial and temporal densities of wind data, errors in the observation and analysis, and assumptions used in the calculations.

Large uncertainties in the diagnostic trajectories have been suggested by several studies using the tetroon technique (Hoecker, 1977; Pack et al., 1977; Clarke et al., 1983) and the tracer technique (Draxler, 1987; Haagenson et al., 1987). These studies indicate that the accuracy of a trajectory model varies significantly with the meteorological situation. Hoecker (1977) found that mean trajectory errors by different models and meteorological conditions ranged from 1 to 42% of trajectory

* Corresponding author.
E-mail address: lty@atmos.yonsei.ac.kr

length. Clarke et al. (1983) indicated that the mean relative error was smaller for days with well-defined flow regimes than that for days with ill-defined flow regimes. Kahl and Samson (1986), using the meteorological data collected during the Cross Appalachian Tracer Experiment (CAPTEX) (Ferber et al., 1986), found that the boundary layer trajectories calculated using data from the US National Weather Service upper-air observation network with a 12-h temporal resolution contained a 50% chance of horizontal transport error exceeding 350 km after 72 h of travel.

The observing system simulation technique (OSST) has been used by several researchers to investigate the accuracy and sensitivity of trajectory models (Kuo et al., 1985; Rolph and Draxler, 1990; Doty and Perkey, 1993). In these studies, the wind fields produced by a numerical weather prediction model are used as "true" or reference meteorological fields, which are then used to generate the reference trajectories and lower resolution wind data. Kuo et al. (1985), through their observing system simulation experiments for a 3-day period case under a mostly cyclonic flow condition, indicated that the synoptic network and observational frequency over North America were inadequate for accurate computation of long-range transport of episodic events and that improvement in trajectory accuracy could be achieved more effectively by enhancing the temporal frequency of observations rather than the spatial resolution.

Some different findings have been reported concerning the effectiveness of the density increase of wind data for the improvement of the trajectory accuracy. Kahl and Samson (1986) found that an increase of spatial density improved the accuracy more than an increase of temporal density. Draxler (1987), who used both meteorological and concentration data obtained during CAPTEX, suggested that the enhancement of the temporal resolution increased the trajectory accuracy, but the improvement was not significantly different from that by enhancing the spatial resolution. On the other hand, Rolph and Draxler (1990) found that the greatest improvement in trajectory accuracy could be achieved by enhancing the temporal frequency of observations to a 6-h interval, if rawinsonde observations were the primary source of meteorological data. Kahl and Samson (1986) attributed the relatively weaker sensitivity of transport error to the spatial density in Kuo et al.'s (1985) results to the fairly homogeneous wind within flow regimes, while Rolph and Draxler (1990) pointed out that the results of Kahl and Samson (1986) were based on the trajectories under generally persistent flow conditions.

Estimated accuracy and sensitivity of trajectory models may depend on the resolution of the reference (or "true") meteorological data used for the trajectory calculations, when the OSST is employed for the sensitivity study. Kuo et al. (1985) and Rolph and Draxler (1990) used the wind fields from 80- and 90-km grid models, respectively, as the reference fields. These were considered to be as high resolution data at the time of those studies. Meteorological fields produced by models with such grid sizes may contain significantly weaker vertical motion and mesoscale variability than those of the real fields. Consequently, the absolute accuracy of a trajectory model will be greater with such reference wind fields than what would be obtained with higher resolution reference wind fields. The effectiveness of data density increase on the improvement of trajectory accuracy may also depend on the resolution of reference fields, to some extent, as well as on the meteorological situation.

The target area of the studies mentioned above is the North American continent. These types of studies have not yet been reported for the eastern Asian region where the long-range transport of air pollutants is becoming a more important environmental problem and where the trajectory method is frequently used to find source–receptor relationships. This region is characterized by mountainous areas and notable land/sea thermal contrast, which may force significant mesoscale variability in both cold and warm seasons. The trajectories calculated using synoptic data in this region may contain significant error, and their accuracy needs to be evaluated using the wind data with resolution fine enough to resolve mesoscale features and diurnal variations of meteorological fields.

This study attempts to evaluate the dependence of three-dimensional (3D) trajectories on the temporal and spatial densities of wind data by applying OSST to three meteorological cases over eastern Asia. Accuracy of an isobaric trajectory model is also discussed. A numerical atmospheric model is employed to generate the reference atmospheric fields with a horizontal grid size of 20 km. The experimental design and methods are given in Section 2. In Section 3, simulated reference meteorology and reference trajectories are introduced. The sensitivity of 3D trajectories to the spatial and temporal densities of wind data is evaluated in Section 4, and the accuracy of isobaric trajectories is described in Section 5. Finally, the summary and conclusions are given in Section 6.

## 2. Experiments

The experiment discussed here consists of the generation of meteorological data sets, calculations of the 3D and 2D trajectories, and error analysis of the calculated trajectories. Three-dimensional meteorological fields generated by a high resolution model are assumed to be the reference fields and the trajectories obtained using the reference fields are assumed to be the reference trajectories. The meteorological data sets with various spatial and temporal densities are then obtained from the reference fields and are used to produce 3D and 2D trajectories. Accuracy and sensitivity of these trajectories are evaluated by comparing them to the reference trajectories.

### *2.1. Generation of meteorological fields*

This study employs RAMS mesoscale model of Colorado State University (Tripoli and Cotton, 1982; Tremback et al., 1985) to generate the reference meteorological fields. The model used in this study assumes a hydrostatic atmosphere on a terrain-following sigma-z coordinate. A Smagorinsky-type eddy coefficient is used for eddy diffusion and a simplified Kuo-type parameterization is used for cumulus convection (Tremback, 1990). The Davies nudging method is used for the lateral boundary conditions and ground-surface temperature is predicted using the soil model of Tremback and Kessler (1985).

The model domain covers the eastern Asian region as shown in Fig. 1, and the horizontal grid size is 20 km. Numerical integrations are carried out for 48 h for each meteorological episode. The meteorological episodes are from three seasons: 13–15 February 1986 (case 1), 30 March–1 April 1993 (case 2) and 9–11 July 1989 (case 3) (Table 1). Important meteorological features of each case will be described in Subsection 3.1.

The reference horizontal wind fields, in which $u$ and $v$ are spatially staggered on the Arakawa-C grid, are first placed on the same grid point (the center of the 20 km grid). The relocated 20-km grid data are stored every hour and are then used to generate the 1 hourly simulated observations with various spatial densities ($\Delta x = 40$, 80, 160, 320 km) by simply selecting the data with the respective space intervals. After meteorological fields with various spatial densities are obtained, vertical velocities are computed using the anelastic continuity equation. The horizontal and vertical velocities with different spatial densities are then all interpolated onto the 20-km grids using a cubic spline interpolation method (Akima, 1970). To calculate 2D trajectories, the reference fields are used to generate the wind fields on the isobaric surfaces (925-, 850-, and 700-hPa surfaces) and isentropic surfaces with various spatial densities at a 6-hour interval, which are also interpolated onto the 20-km grids.

### *2.2. Calculation of trajectories*

The reference trajectories are obtained within the prediction model. The trajectories are integrated every 5 min with an explicit integration:

$$X(t+\Delta t) = X(t) + V(X, t)\, \Delta t \tag{1}$$

where

$$X = X(x, y, z^*), \quad V = V(u, v, w^*)$$

at location $X$ and time $t$, $\Delta t$ is the time step, $u$ and $v$ are the wind speeds in the $x$ and $y$ directions, respectively, and $w^*$ is the vertical velocity on the terrain-following coordinate ($z^*$):

$$z^* = s\,\frac{z - z_g}{s - z_g}, \tag{2}$$

where $s$ is the height of the model top, $z_g$ is the ground-surface height, and $z$ is the height above sea level. The turbulent fluctuation is not considered in the trajectory calculation.

The integration of the trajectory starts 12 hours into the meteorological simulation, when the model-produced meteorological fields are spin up and contain mesoscale features. The particles are initially located on constant pressure surfaces at the 925-, 850- and 700-hPa levels. Thus their initial heights on the terrain-following coordinate may

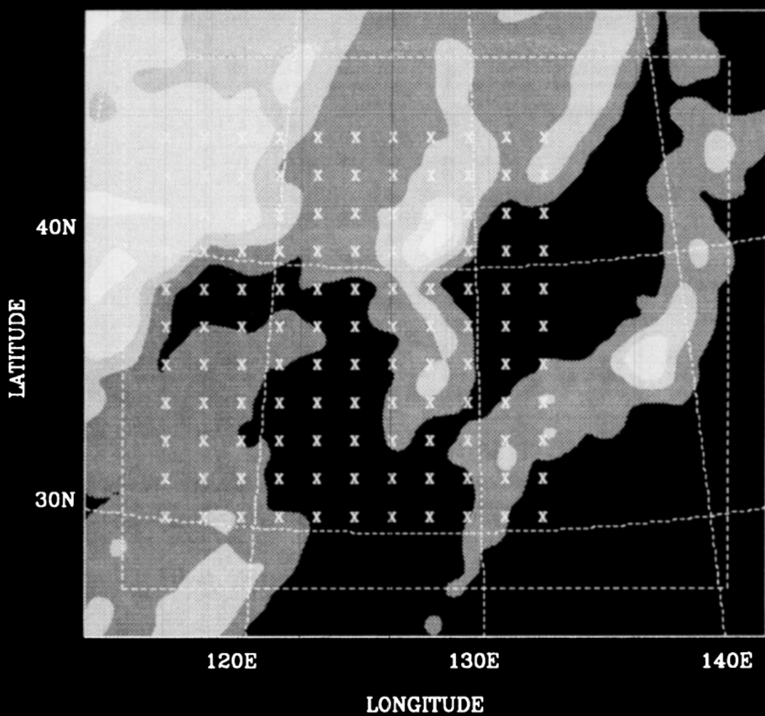


*Fig. 1.* Smoothed topography in the domain for the meteorological simulations and the initial horizontal locations of particles which are marked by crosses. Terrain heights of 50 m, 500 m, 1000 m, and 1500 m are shaded with increasing darkness. The inner square represents the trajectory domain.

Table 1. *Summary of the meteorological episodes*

| | Period | Meteorological features |
|---|---|---|
| case 1 | 12 UTC 13 February– 12 UTC 15 February 1986 | southeastward excursion of Siberian high; strong baroclinicity in the lower troposphere |
| case 2 | 00 UTC 30 March– 00 UTC 1 April 1993 | passage of a synoptic scale cyclone across the model domain; yellow sand transport over the eastern Asia |
| case 3 | 12 UTC 9 July– 12 UTC 11 July 1989 | meso-α-scale cyclone and heavy rainfall associated with the Changma (monsoon) front; importance of diurnal and condensational heating |

not be the same. There are 121 particles at each level with the horizontal distance of 160 km between particles as shown in Fig. 1. The initial heights of several particles are below or very near the ground surface, especially for the 925-hPa particles. These particles are discarded. When a particle exits the trajectory domain, it is also discarded. The trajectory domain is smaller than the domain for the meteorological simulation as shown by the smaller square in Fig. 1.

To investigate the sensitivity of trajectories to the spatial and temporal densities of wind data, 3D trajectories are computed from (1) using the wind data sets with various combinations of data densities in space ($\Delta x = 20$, 40, 80, 160, 320 km) and time (1, 3, 6, 12 hourlies). The horizontal and vertical velocities at the location of a trajectory particle are linearly interpolated in time and space. 2D trajectories are obtained by the same explicit integration using 6 or 12 hourly horizontal winds.

The time step for these trajectory calculations is also 5 min.

### 2.3. *Transport error*

The error in a trajectory is represented in terms of absolute and relative transport errors as in Kuo et al. (1985). The mean absolute transport errors are represented by $E_H$ and $E_V$ for horizontal and vertical directions, respectively:

$$E_H(t) = \frac{1}{N}\sum_{n=1}^{N} [(x_r^{(n)}(t) - x_c^{(n)}(t))^2 + (y_r^{(n)}(t) - y_c^{(n)}(t))^2]^{1/2}, \quad (3)$$

$$E_V(t) = \frac{1}{N}\sum_{n=1}^{N} |z_r^{(n)}(t) - z_c^{(n)}(t)|, \quad (4)$$

where $N$ is the number of particles, and the subscripts r and c indicate the reference and computed particle locations, respectively, and the superscript $n$ denotes the $n$th particle.

Relative mean transport errors are defined by the following:

$$RE_H(t) = \frac{E_H(t)}{D_H(t)}, \quad (5)$$

$$RE_V(t) = \frac{E_V(t)}{D_V(t)}, \quad (6)$$

where $D_H$ and $D_V$ are the mean absolute transport distances of a reference case in the horizontal and vertical directions, respectively. They are defined as

$$D_H(t) = \frac{1}{N}\sum_{n=1}^{N} [(x_r^{(n)}(t) - x_r^{(n)}(t_0))^2 + (y_r^{(n)}(t) - y_r^{(n)}(t_0))^2]^{1/2}, \quad (7)$$

$$D_V(t) = \frac{1}{N}\sum_{n=1}^{N} |z_r^{(n)}(t) - z_r^{(n)}(t_0)|, \quad (8)$$

where $x_r^{(n)}(t_0)$, $y_r^{(n)}(t_0)$, $z_r^{(n)}(t_0)$ describe the initial location of the $n$th particle.

## 3. Reference fields

### 3.1. *Reference meteorology*

The sea-level pressure patterns for the three cases are presented in Fig. 2 to show the characteristic features of the reference meteorology in each case. In case 1, the Siberian High makes gradual southeastward excursion producing a strong east-west pressure gradient around the Korean peninsula (Figs. 2a, b). At 00 UTC 15 February 1986, the high pressure system is located in northern China and eastern Mongolia (northwestern part of the domain) and a low pressure system is found over and to the east of Japan. In case 2, a synoptic-scale low pressure system dominates the region throughout the integration period (Figs. 2c, d). A well-developed cyclone is over the east Asian continent at 12 UTC 30 March 1993. It moves southeastward and weakens with time. Significant mesoscale variabilities are found around the mesoscale mountains in the northern Korean peninsula. Case 3 is characterized by strong convection and heavy rainfall associated with the Changma (monsoon) front (Figs. 2e, f). A synoptic scale low pressure system is over Manchuria. A mesoscale low, which produces heavy rainfall, is near the west coast of the peninsula at 00 UTC 11 July 1989 and moves eastward developing further. Comparison of these simulated reference fields with the actual observations (not shown) indicates that both the synoptic- and meso-scale features of the simulated fields are in good agreement with those of observations. Important mesoscale features include the mesoscale trough over the Korean peninsula in case 1 and the meso-$\alpha$-scale low in case 3. These fair agreements between the observed and the simulated reference fields support the applicability of the current results to the real atmosphere.

The three cases show differences in the movement of the pressure system. In case 1, the high pressure system gradually moves southeastward, thus the change of the general flow pattern with time is relatively slow. On the other hand, the synoptic scale low in case 2 is moving southeastward relatively fast, and consequently temporal variations of the low-level airflow in this case are relatively large. In case 3, the synoptic scale low does not move significantly, but the meso-$\alpha$-scale low is moving quickly eastward.

Another important difference between the cases is in the strength of baroclinicity. Although not shown here, baroclinicity is strong in case 1 and relatively weak in case 3. Average values of vertical wind shear between the 925- and 700-hPa levels are 5.0, 3.3 and 2.6 $\mathrm{m\,s^{-1}}$ $(100\ \mathrm{mb})^{-1}$ for cases 1, 2 and 3, respectively. The vertical wind shear is

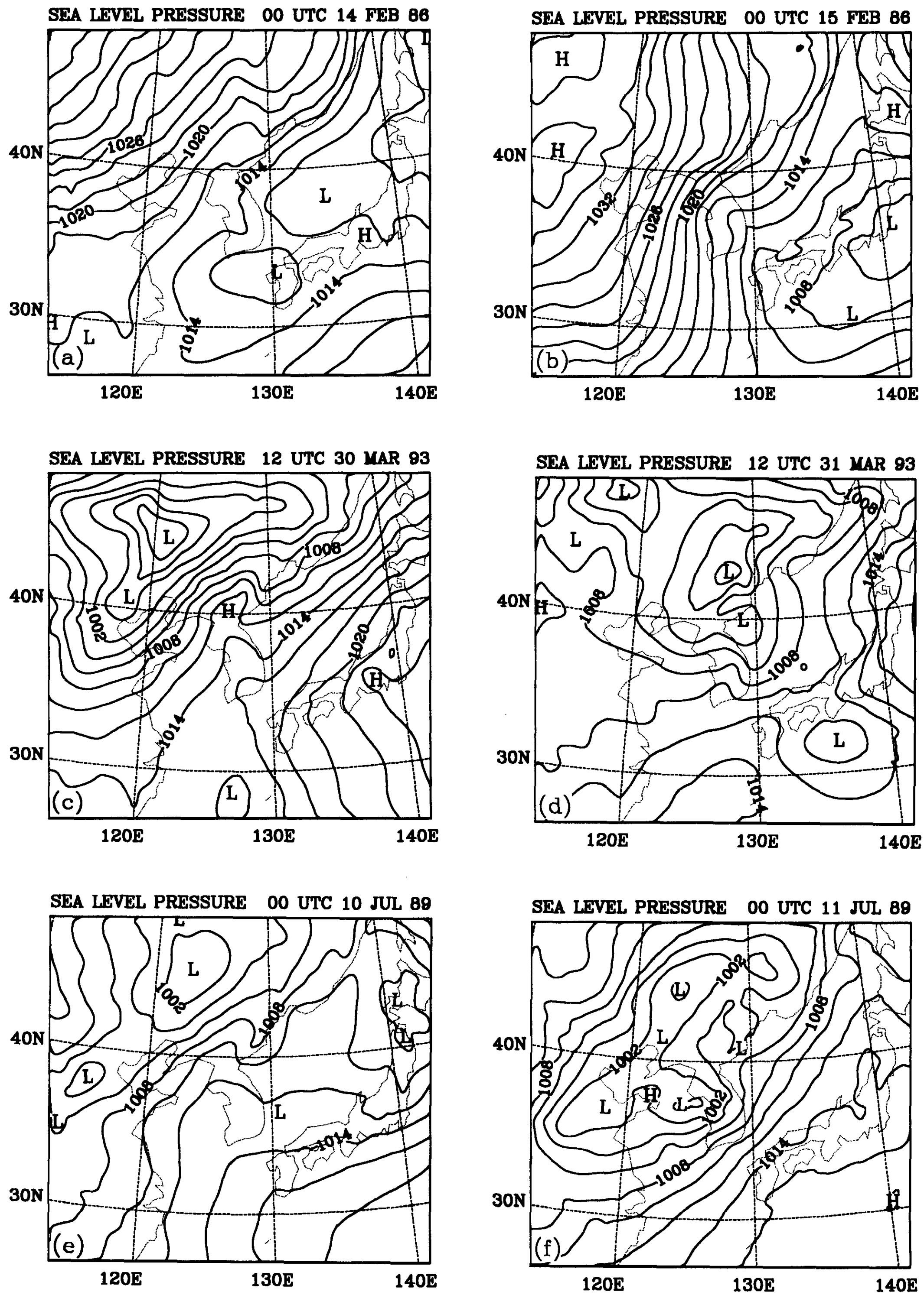


*Fig. 2.* Sea-level pressure charts for case 1 (a, b), case 2 (c, d) and case 3 (e, f).

defined as $((\Delta u/\Delta p)^2+(\Delta v/\Delta p)^2)^{1/2}$. These values are the time and domain averages of the 20-km grid values at 6-h intervals for the 36-h period of trajectory integration.

### *3.2. Reference trajectories*

Reference trajectories of the 850-hPa particles are shown in Fig. 3. Both the plane and 3D views of the trajectories are shown. In case 1, the particles initially over the northwestern part of the domain tend to move southward and downward (Figs. 3a, b). On the other hand, particles in the southeastern part tend to move horizontally eastward. The particles in the area over the surface low to the east of the Korean peninsula show complicated patterns of trajectories with some upward displacements.

Trajectories in cases 2 and 3 are more scattered vertically than those in case 1. A significant portion of the particles in case 2 show northeastward movement following the airflow associated with the synoptic scale cyclone (Figs. 3c, d). In case 3, some particles above the region of strong convection rise higher than 10 km and then are transported southeastward by the upper-level wind, while most of the particles at lower levels are transported northeastward or eastward (Figs. 3e, f). Trajectories for the 925- and 700-hPa particles (not shown) also exhibit similar characteristic behaviors of each case described above, although differences are found in some features such as horizontal and vertical travel distances.

The number of particles that exit the model domain increases with time. For the 925-hPa particles, 63, 85 and 84 of them remain in the domain after 24 h of travel for cases 1, 2 and 3, respectively, while 27, 72, and 63 particles still remain in the domain after 36 hours of travel. In the case of 700-hPa particles, 79, 90 and 82 of them remain in the domain after 24 h for cases 1, 2 and 3, respectively, and 32, 67 and 32 of them remain in the domain after 36 h.

## 4. Sensitivity of 3D trajectories to the spatial and temporal densities of wind data

The mean absolute transport errors after 24 h of travel for the 925-hPa particle trajectories are shown in Fig. 4 as a function of temporal density. The error generally increases as the data density decreases. The sensitivity of $E_H$ to the temporal density gradually decreases as the space interval of the wind data increases. This is mainly due to the relatively large growth of $E_H$ with an increase in the space interval for trajectories from 1 and 3 hourly data sets. As a result, the sensitivity to the temporal density change between 6- and 12-h intervals becomes more pronounced as the space interval of the wind data increases. When data sets with a 320-km interval are used, the trajectories are not sensitive to the temporal density change between 1- and 6-h intervals in all three cases, and also between 6- and 12-h intervals in case 1. The trajectories are also sensitive to the spatial density. The general manner for the dependence of $E_H$ on the spatial density is similar to that on the temporal density. $E_H$ is highly sensitive to the spatial density change between 160- and 320-km intervals.

Values of $E_V$ are significantly smaller for case 1 than those in cases 2 and 3. $E_V$ exhibits some sensitivity differences between the cases. Its sensitivity to the temporal density is especially weak in case 1, but is strong in case 2 for which the sensitivity is linear. In case 3, $E_V$ is highly sensitive only for the high spatial and temporal densities. Its sensitivity to the spatial density change between 160- and 320-km intervals is much weaker than that of $E_H$.

For the 850-hPa particle trajectories (Fig. 5), the sensitivity to the data density is similar to that for the 925-hPa particle trajectories. The relatively strong sensitivity to the temporal density change between 6- and 12-h intervals is similarly found. However, the sensitivity to the spatial density change between the 160- and 320-km intervals is weaker for the 850-hPa particle trajectories. In case 3, trajectories from data sets with the space interval of 20–80 km show very strong sensitivity to the temporal density. For the 700-hPa particle trajectories (Fig. 6), case 1 shows relatively strong sensitivity to the spatial density change between 160- and 320-km intervals.

These figures show that the 3D trajectories are sensitive to both the temporal and spatial densities of wind data. The sensitivity is found to vary with the case and the initial height of particles. Trajectories in case 1 are less sensitive to the temporal density than those in cases 2 and 3. The trajectories show relatively stronger sensitivity to the temporal density change between 6- and 12-h

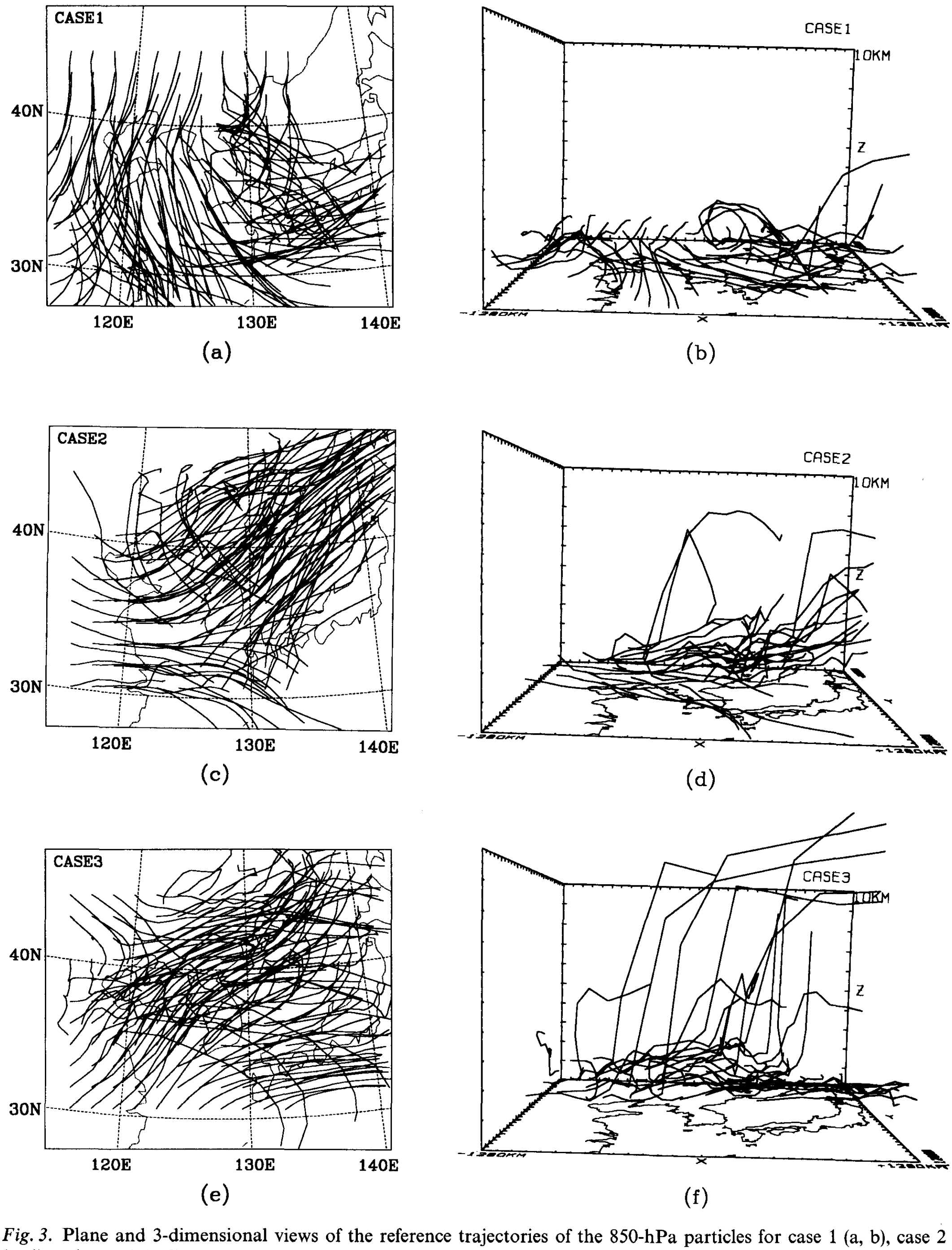


*Fig. 3.* Plane and 3-dimensional views of the reference trajectories of the 850-hPa particles for case 1 (a, b), case 2 (c, d) and case 3 (e, f).

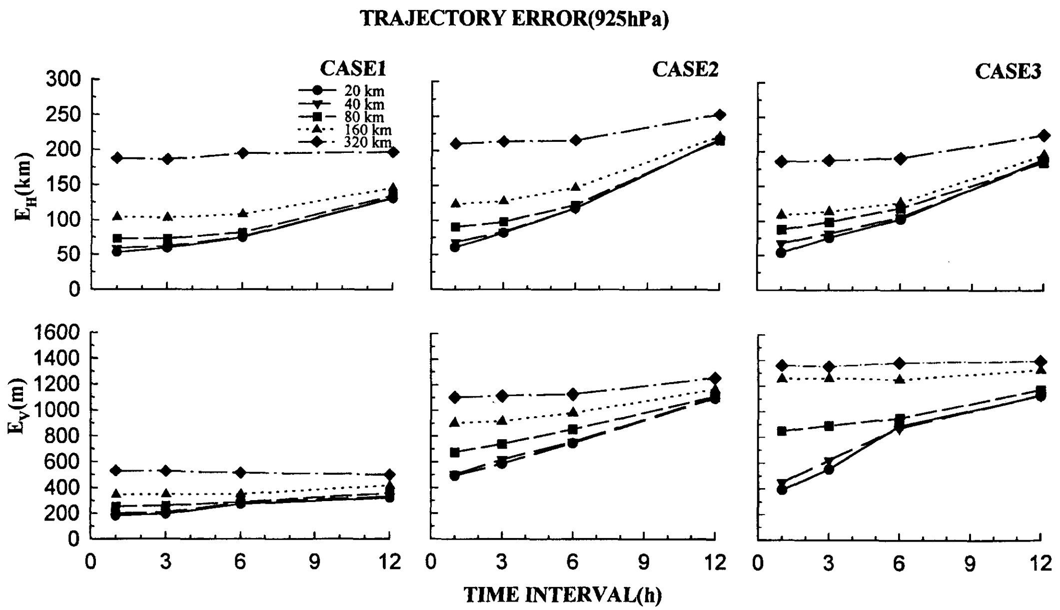


*Fig. 4.* Mean absolute transport errors after 24 h of travel for the 925-hPa particle trajectories as a function of the time interval of wind data.

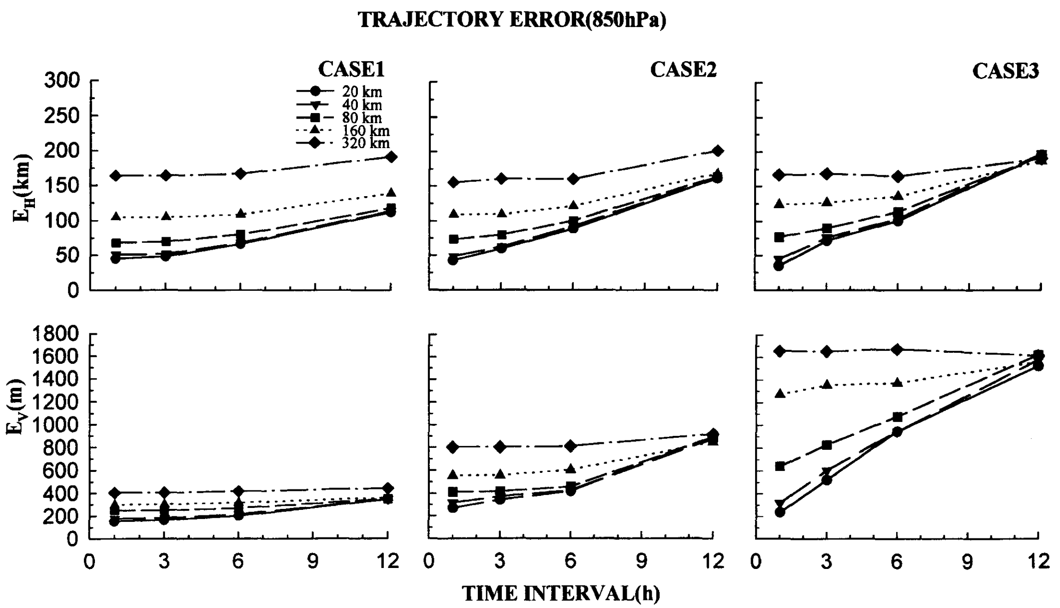


*Fig. 5.* Same as Fig. 4, except for the 850-hPa particle trajectories.

intervals in general and to the spatial density change between 160- and 320-km intervals in case 1. The sensitivity to the spatial density change between 160- and 320-km intervals is stronger for the 925-hPa particle trajectories than those for the 850- and 700-hPa particle trajectories. This may be explained by the decrease of mesoscale variability in the air flow with the height. The

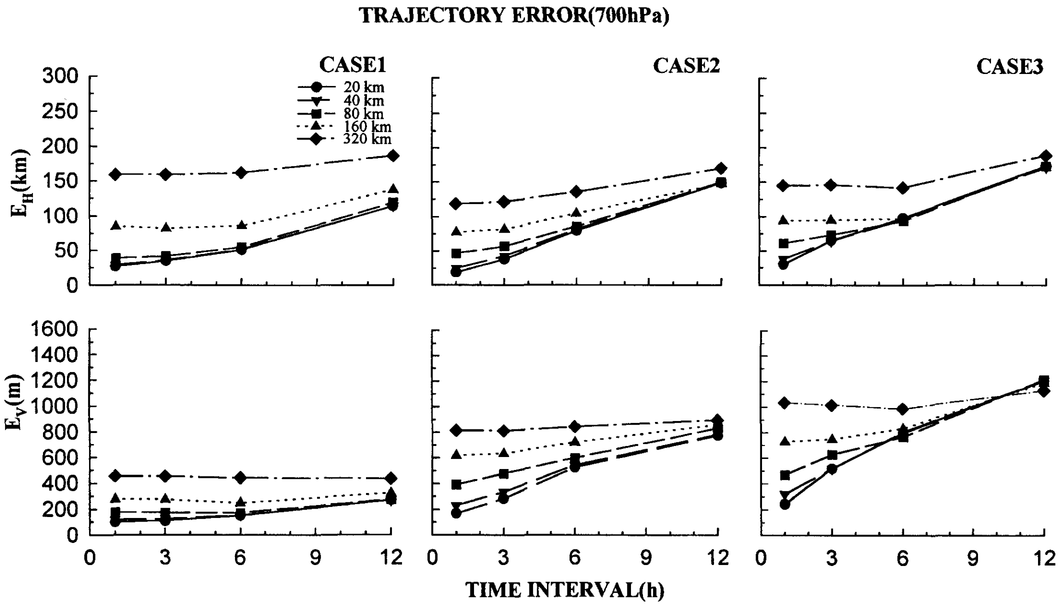


*Fig. 6.* Same as Fig. 4, except for the 700-hPa particle trajectories.

present results also indicate the importance of balance between the temporal and spatial densities for the effective achievement of better accuracy in trajectory calculations. The coarse resolution in either the temporal or spatial sampling may contribute most of the transport errors.

Temporal variations of mean absolute transport error for the trajectories from wind data sets with 12-h and 320-km intervals are shown for the 925-hPa particles in Fig. 7. $E_H$ increases with time in an approximately linear manner. Rate of error growth is relatively large for case 2 throughout the integration. The large growth rate in case 1 after 24 h of travel appears to be caused by the strong vertical wind shear. Significant differences between the cases are found in the variation of $E_V$. $E_V$ increases with time in an approximately linear manner in case 2, while it increases rapidly during the period of 9–18 h and then changes slowly afterwards in case 3. In case 1, it slowly

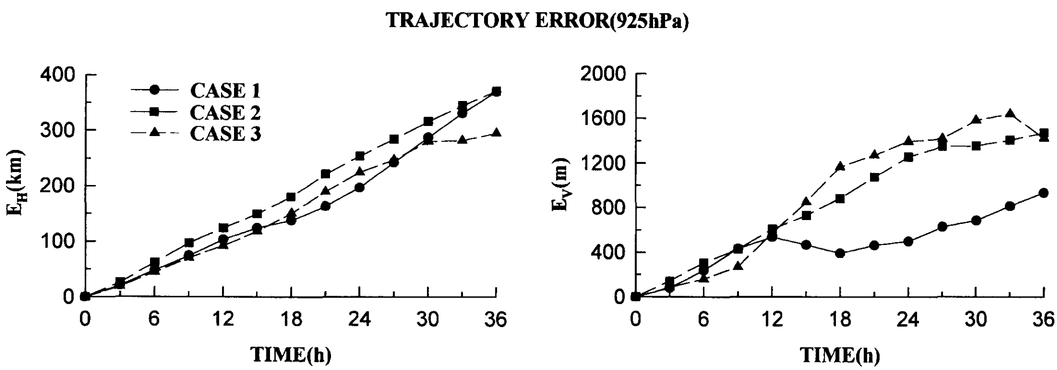


*Fig. 7.* Temporal variations of mean absolute horizontal and vertical transport errors for the 925-hPa particle trajectories which are calculated using wind data sets with 12-h, 320-km resolution.

increases with time initially and remains steady after 12 h until it increases again after 24 h of trajectory integration.

Relative mean transport errors vary slowly with time in general and show steady patterns as shown in Fig. 8 for the 925-hPa particle trajectories. Table 2 shows the relative mean transport errors averaged over the period of 24–36 h of travel. The magnitude of $RE_H$ decreases with increasing initial particle height. When data sets with 12-h and 320-km intervals are used, the values of $RE_H$ for case 1 are the largest among the three cases (0.36, 0.30 and 0.21 for 925-, 850- and 700-hPa particle trajectories, respectively). The corresponding values for cases 2 and 3 are identical or close to each other (0.30, 0.23–0.25 and 0.19 for 925-, 850-and 700-hPa particle trajectories, respectively). However, when a 12-hourly data set with a 40- or 80-km spatial resolution is used as an example, $RE_H$ for case 1 is the smallest among the three cases. This may be explained by the difference in the accuracies of vertical velocities obtained from horizontal winds with different spatial densities in a relatively persistent synoptic weather system with strong vertical shear of horizontal winds in case 1. Use of inaccurate vertical velocities can give very large transport errors in such situations. These results indicate that vertical shear of horizontal winds may be the primary factor for determining the accuracy of trajectory calculations when wind data sets with low data density are used.

According to Figs. 4–6 and Table 2, the effectiveness of enhancing the temporal or spatial resolution of wind data for the improvement of trajectory accuracy varies with the meteorological situation. When the intervals of 12 h and 320 km are assumed to be the resolution of wind observations, increasing the spatial density improves the accuracy more than increasing the temporal density in case 1, in which the synoptic scale air flow pattern associated with the Siberian High varies slowly with time. On the other hand, the opposite is true in cases 2 and 3, although the difference in the improvements by the two different enhancements of resolution is small in case 2. Relatively strong sensitivity to the enhancement of temporal resolution in case 3 may be due to the relatively fast movement of the meso-$\alpha$-scale low and diabatic heating.

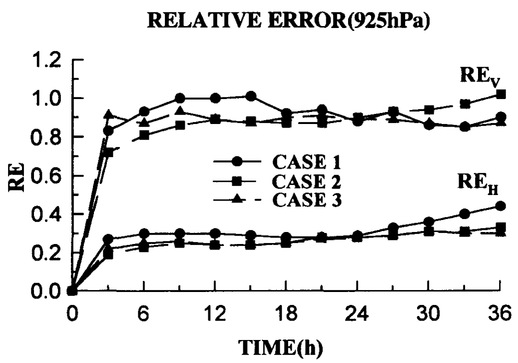


*Fig. 8.* Temporal variations of the relative mean horizontal and vertical transport errors for the 925-hPa particle trajectories which are calculated using wind data sets with 12-h, 320-km resolution.

The present results are to some extent consistent with both Kahl and Samson (1986) and Kuo et al. (1985). Kahl and Samson suggested that enhancing the spatial resolution improves the trajectory accuracy more than enhancing the temporal resolution when considering a relatively persistent flow condition. Kuo et al. found that enhancing the temporal resolution is more effective, based on the results for a case with a cyclonic flow condition.

The magnitudes of transport errors found in this study, however, are larger in general than those obtained by the previous studies. When data sets with 12-hour and 320-km intervals are used for the trajectories of particles initially located at 925-hPa, the values of $E_H$ at 24 h of travel are in the range of 197–254 km in the present study. Rolph and Draxler (1990) obtained 186 km for $E_H$ at 24 h for all synoptic conditions during a 74-day period, using data sets with 12-h and 360-km intervals for the particles initially located at $\sigma = 0.95$. Kuo et al. (1985), using data sets with 12-h and 320-km intervals, obtained smaller absolute transport errors for particles initially at $\sigma = 0.945$ than those of Rolph and Draxler. These two studies used reference wind fields from an 80- or 90-km grid model.

The magnitude of transport error may depend on the structure of reference wind fields to some extent. The reference fields obtained from a 20-km grid model may contain stronger mesoscale variation of horizontal wind and stronger vertical motion within a disturbance area than those obtained from a model with a larger grid (i.e., 80-km grid). To investigate the impacts of reso-

Table 2. *Relative mean transport error averaged over the period of 24–36 h of travel*

| | | 1 hourly | | | | 6 hourly | | | | 12 hourly | | | |
|---|---|---|---|---|---|---|---|---|---|---|---|---|---|
| | | 40 km | 80 km | 160 km | 320 km | 40 km | 80 km | 160 km | 320 km | 40 km | 80 km | 160 km | 320 km |
| *925-hPa particle trajectory* | | | | | | | | | | | | | |
| case 1 | $RE_H$ | 0.14 | 0.17 | 0.22 | 0.36 | 0.16 | 0.18 | 0.22 | 0.36 | 0.24 | 0.23 | 0.27 | 0.36 |
| | $RE_V$ | 0.44 | 0.48 | 0.67 | 0.88 | 0.54 | 0.56 | 0.64 | 0.89 | 0.67 | 0.64 | 0.72 | 0.88 |
| case 2 | $RE_H$ | 0.10 | 0.13 | 0.17 | 0.27 | 0.16 | 0.17 | 0.19 | 0.27 | 0.27 | 0.27 | 0.28 | 0.30 |
| | $RE_V$ | 0.44 | 0.49 | 0.68 | 0.86 | 0.56 | 0.63 | 0.75 | 0.86 | 0.87 | 0.87 | 0.90 | 0.95 |
| case 3 | $RE_H$ | 0.09 | 0.13 | 0.17 | 0.25 | 0.16 | 0.18 | 0.18 | 0.25 | 0.28 | 0.28 | 0.27 | 0.30 |
| | $RE_V$ | 0.37 | 0.54 | 0.75 | 0.85 | 0.56 | 0.62 | 0.82 | 0.86 | 0.85 | 0.84 | 0.89 | 0.87 |
| *850-hPa particle trajectory* | | | | | | | | | | | | | |
| case 1 | $RE_H$ | 0.10 | 0.13 | 0.16 | 0.25 | 0.12 | 0.14 | 0.16 | 0.25 | 0.18 | 0.18 | 0.20 | 0.30 |
| | $RE_V$ | 0.44 | 0.52 | 0.69 | 0.78 | 0.48 | 0.56 | 0.73 | 0.78 | 0.73 | 0.75 | 0.75 | 0.82 |
| case 2 | $RE_H$ | 0.07 | 0.09 | 0.13 | 0.18 | 0.11 | 0.12 | 0.14 | 0.18 | 0.20 | 0.20 | 0.20 | 0.23 |
| | $RE_V$ | 0.29 | 0.41 | 0.55 | 0.83 | 0.47 | 0.50 | 0.59 | 0.84 | 0.88 | 0.87 | 0.86 | 0.96 |
| case 3 | $RE_H$ | 0.07 | 0.11 | 0.18 | 0.22 | 0.16 | 0.17 | 0.19 | 0.22 | 0.28 | 0.28 | 0.27 | 0.25 |
| | $RE_V$ | 0.24 | 0.41 | 0.69 | 0.85 | 0.52 | 0.60 | 0.73 | 0.85 | 0.98 | 0.97 | 0.91 | 0.87 |
| *700-hPa particle trajectory* | | | | | | | | | | | | | |
| case 1 | $RE_H$ | 0.04 | 0.06 | 0.10 | 0.19 | 0.07 | 0.07 | 0.10 | 0.19 | 0.13 | 0.14 | 0.16 | 0.21 |
| | $RE_V$ | 0.25 | 0.33 | 0.47 | 0.79 | 0.33 | 0.34 | 0.47 | 0.77 | 0.51 | 0.52 | 0.59 | 0.81 |
| case 2 | $RE_H$ | 0.03 | 0.06 | 0.10 | 0.14 | 0.09 | 0.10 | 0.12 | 0.16 | 0.17 | 0.17 | 0.17 | 0.19 |
| | $RE_V$ | 0.26 | 0.38 | 0.64 | 0.81 | 0.55 | 0.59 | 0.74 | 0.87 | 0.84 | 0.83 | 0.90 | 0.93 |
| case 3 | $RE_H$ | 0.04 | 0.07 | 0.10 | 0.15 | 0.11 | 0.11 | 0.11 | 0.14 | 0.18 | 0.18 | 0.17 | 0.19 |
| | $RE_V$ | 0.37 | 0.52 | 0.74 | 1.04 | 0.82 | 0.75 | 0.83 | 0.92 | 1.14 | 1.13 | 1.09 | 0.96 |

lution of reference wind data on the accuracy estimate and sensitivity of 3D trajectories, further experiments have been performed using wind data sets with the 1-h, 80-km grid resolution as the reference fields. The reference fields are selected from the 20-km grid data sets and are spatially smoothed by a 9-point, 2-dimensional smoother to eliminate the high frequency wave component which an 80-km grid can not resolve properly. Wind data sets with lower spatial densities (160- and 320-km intervals) are obtained from these reference data sets and then interpolated to the 80-km grids using a cubic spline interpolation. Trajectories are calculated using these wind data sets. The trajectories obtained using the reference wind fields with the 1-h, 80-km grid resolution are assumed to be the reference trajectories. Here we use $E_{H8}$ to denote the mean absolute horizontal transport error against these reference trajectories and $E_{H2}$ for the transport error that has been used in this study.

Table 3 shows the ratio, $E_{H8}/E_{H2}$ after 24 h of travel. The ratio increases with the decrease of data density. When data sets with 12-h and 320-km intervals are used, the ratios are in the ranges of 0.64–0.73, 0.63–0.74 and 0.78–0.91 for 925-, 850- and 700-hPa particle trajectories, respectively. This table indicates that the use of 80-km grid reference wind data in the sensitivity study using OSST can result in a significant underestimation of the transport errors. Kuo et al. (1985) also suggested that the error in their study could be regarded as a lower bound considering the 80-km grid of their reference wind fields.

According to the current study, another important impact of using reference fields with lower resolution is to increase the relative importance of temporal density of wind data. Table 4 shows the ratios of transport errors for the trajectories from the data sets with 6-h, 320-km and 12-h, 160-km resolutions to the error for trajectories from the data sets with 12-h, 320-km resolution: $E_H$ (6 h 320 km)/$E_H$ (12 h 320 km) and $E_H$ (12 h 160 km)/$E_H$ (12 h 320 km). The table indicates that the use of 80-km grid reference fields significantly increases the sensitivity of $E_H$ to the temporal density change between 6- and 12-h intervals. It also increases the sensitivity to the spatial density change between 160- and 320-km intervals, but the increase of sensitivity is generally much smaller than that to the temporal density change. For example, the ratios $E_H$ (6 h 320 km)/$E_H$ (12 h 320 km) and $E_H$ (12 h 160 km)/$E_H$ (12 h 320 km) for the 850-hPa particle trajectories in case 2 are 0.80 and 0.84, respectively, when the spatial interval of the reference wind fields is 20 km, but they are 0.64 and 0.79, respectively, when the spatial interval of the reference fields is 80 km. Table 4 suggests that the use of wind data with 1-h and 80-km intervals as the reference fields may exaggerate the effectiveness of enhancing the temporal resolution for the improvement of trajectory accuracy.

Table 3. *Ratio of the mean absolute horizontal transport errors ($E_{H8}/E_{H2}$) at 24 h of travel; $E_{H8}$ and $E_{H2}$ are as explained in the text*

| | | 6 hourly | | 12 hourly | |
|---|---|---|---|---|---|
| | | 160 km | 320 km | 160 km | 320 km |
| *925-hPa particle trajectory* | | | | | |
| case 1 | $E_{H8}/E_{H2}$ | 0.36 | 0.61 | 0.66 | 0.73 |
| case 2 | $E_{H8}/E_{H2}$ | 0.38 | 0.53 | 0.64 | 0.65 |
| case 3 | $E_{H8}/E_{H2}$ | 0.31 | 0.53 | 0.64 | 0.64 |
| *850-hPa particle trajectory* | | | | | |
| case 1 | $E_{H8}/E_{H2}$ | 0.34 | 0.60 | 0.60 | 0.63 |
| case 2 | $E_{H8}/E_{H2}$ | 0.42 | 0.59 | 0.70 | 0.74 |
| case 3 | $E_{H8}/E_{H2}$ | 0.31 | 0.55 | 0.68 | 0.74 |
| *700-hPa particle trajectory* | | | | | |
| case 1 | $E_{H8}/E_{H2}$ | 0.47 | 0.72 | 0.76 | 0.78 |
| case 2 | $E_{H8}/E_{H2}$ | 0.49 | 0.65 | 0.80 | 0.85 |
| case 3 | $E_{H8}/E_{H2}$ | 0.54 | 0.71 | 0.83 | 0.91 |

Table 4. *Ratios of the transport errors for the trajectories obtained using the data sets with 6-h, 320-km and 12-h, 160-km resolutions to the error for the trajectories from the data set with 12-h, 320-km resolution; the ratio is for 24 h of travel*

| | $\frac{E_{H2}\ (6\ h\ 320\ km)}{E_{H2}\ (12\ h\ 320\ km)}$ | $\frac{E_{H2}\ (12\ h\ 160\ km)}{E_{H2}\ (12\ h\ 320\ km)}$ | $\frac{E_{H8}\ (6\ h\ 320\ km)}{E_{H8}\ (12\ h\ 320\ km)}$ | $\frac{E_{H8}\ (12\ h\ 160\ km)}{E_{H8}\ (12\ h\ 320\ km)}$ |
|---|---|---|---|---|
| *925-hPa particle trajectory* | | | | |
| case 1 | 0.99 | 0.74 | 0.83 | 0.67 |
| case 2 | 0.85 | 0.87 | 0.70 | 0.85 |
| case 3 | 0.85 | 0.87 | 0.71 | 0.87 |
| *850-hPa particle trajectory* | | | | |
| case 1 | 0.87 | 0.73 | 0.83 | 0.69 |
| case 2 | 0.80 | 0.84 | 0.64 | 0.79 |
| case 3 | 0.86 | 0.98 | 0.64 | 0.90 |
| *700-hPa particle trajectory* | | | | |
| case 1 | 0.87 | 0.74 | 0.80 | 0.72 |
| case 2 | 0.80 | 0.87 | 0.61 | 0.81 |
| case 3 | 0.75 | 0.91 | 0.59 | 0.83 |

## 5. Accuracy of isobaric trajectory model

Fig. 9 shows the temporal variation of the transport errors for the isobaric trajectories obtained using the wind data sets with 12-h, 320-km resolution. The horizontal transport error decreases with the trajectory height showing the largest value for the 925-hPa trajectories, except for case 1 in which the 700-hPa trajectories show the largest error during late in the period. At 36 h of travel, the values of $E_H$ for the 925-hPa trajectories are in the range of 353–406 km. The values of the relative mean horizontal transport error averaged over 24–36 hours of travel are in the ranges of 0.32–0.39, 0.26–0.34 and 0.20–0.28 for the 925-, 850- and 700-hPa particle trajectories, respectively (not shown).

The rapid growth of $E_V$ for the 700-hPa trajectories in case 1 correlates well with that of $E_H$, indicating the importance of vertical transport error for the accuracy of trajectories in a situation with strong vertical wind shear. This large increase of error in case 1 is associated with the particles which are initially located in the northwestern part of the model domain (the eastern part of the Siberian High) and show southward and downward transports under synoptic conditions of strong vertical variation of horizontal winds. Isobaric trajectories for those particles show southward transports during the early period but eastward transports during the middle and late in the period.

When data sets with 12-h, 320-km resolution are used for the calculation of trajectories, the mean transport errors of the isobaric trajectories are comparable to those of 3D trajectories, although the isobaric trajectories contain larger error (Table 5). The ratio of the isobaric trajectory error to the 3D trajectory error does not change very much with time in general. Its values for $E_H$ averaged over the period of 24–36 h of travel are in the range of 1.03–1.22 except for the 700-hPa particle trajectories in case 1 for which the ratio is 1.33. According to the current results, the isobaric model can give a very large trajectory error under a strongly baroclinic condition.

The effectiveness of enhancing either temporal or spatial resolution of wind data for the improvement of isobaric trajectory accuracy shows the same dependence on the meteorological situation as that found for the 3D trajectories. However, the improvements in the accuracy of the isobaric

Table 5. *Average ratio of mean absolute transport errors for the isobaric and 3D trajectories ($E_H(2D)/E_H(3D)$) obtained using data sets with 12-h, 320-km resolution; the average is for the period of 24–36 h of travel*

| | 925 hPa | 850 hPa | 700 hPa |
|---|---|---|---|
| case 1 | 1.04 | 1.19 | 1.33 |
| case 2 | 1.03 | 1.08 | 1.03 |
| case 3 | 1.22 | 1.14 | 1.04 |

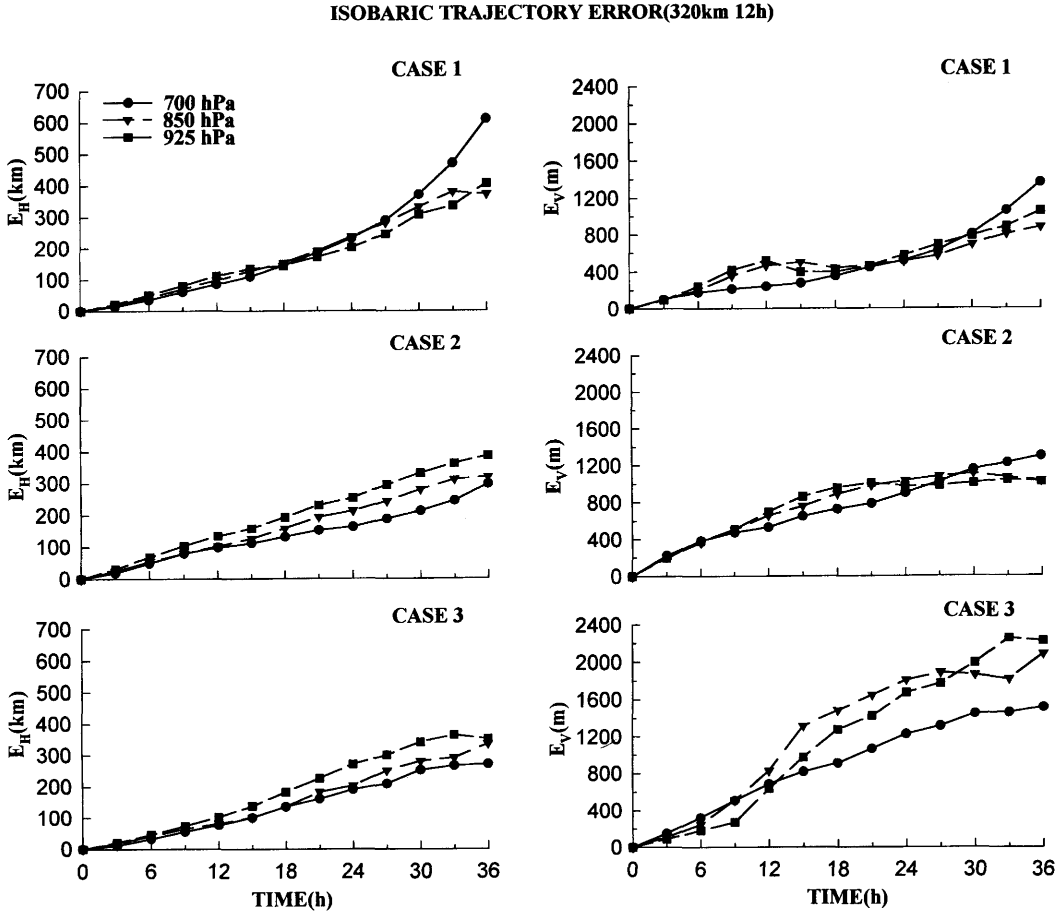


*Fig. 9.* Temporal variations of the mean absolute horizontal and vertical transport errors for the isobaric trajectories which are calculated using wind data sets with 12-h, 320-km resolution.

trajectories by increasing the data density are generally less than those found for the 3D trajectories. For example, the values of the ratio, $E_H$ (6 h 320 km)/$E_H$ (12 h 320 km) for the isobaric trajectories are in the ranges of 0.91–0.97, 0.86–0.95 and 0.78–0.86 for the 925-, 850- and 700-hPa trajectories, respectively.

Accuracy of isentropic trajectory model is not discussed in this paper, since the use of isentropic model is found to be severely limited for particles at lower levels in cases 1 and 2. Most or a major portion of the particles in case 1, and a significant portion of the 925- and 850-hPa particles on isentropic surfaces in case 2 are discarded during the trajectory integration. In the wintertime case (case 1), mixed layers can be found over the land during daytime and also over the warmer seas as the colder air from the Asian continent outbreaks over the sea. Furthermore, the atmosphere is strongly baroclinic so that the isentropic surfaces significantly slope down to the south. In such a situation, the particles moving southward on isentropic surfaces will reach lower level soon and most of them will exit the domain moving further southward and downward. However, the large difference in the number of remaining particles between the isentropic and the 3D trajectories does not necessarily mean that the isentropic trajectories are very different from the 3D trajectories. The reference trajectories tend to show isentropic behaviors unless they are within the area of diabatic heating (e.g., surface sensible heating and condensational heating, etc.). According to the 700-hPa particle trajectories, the isentropic model performs much better than the isobaric model in cases 1 and 2, while the two models perform comparably in case 3.

## 6. Summary and conclusions

An investigation has been carried out to evaluate the dependence of trajectory accuracy on the density of wind data. The present study has applied the observing system simulation technique to three meteorological cases over the east Asian region. It has employed CSU RAMS to generate the reference atmospheric fields with a horizontal grid size of 20 km. The three meteorological cases can well be distinguished from each other by their characteristic features: excursion of a Siberian High and strong vertical wind shear in case 1, a synoptic scale low and its associated cyclonic circulation in case 2, and low pressure systems and impacts of condensational and diurnal heating on the air flow in case 3.

3-dimensional trajectories are sensitive to both the temporal and spatial densities. The trajectories show relatively strong sensitivity to the temporal density change between 6-and 12-h intervals in general, and also to the spatial density change between 160- and 320-km intervals in one of the cases. Sensitivity to the spatial density change between 160- and 320-km intervals is stronger for the 925-hPa particle trajectories than those for the 850- and 700-hPa particle trajectories. When data sets with 12-hour and 320-km intervals are used, the relative mean horizontal transport errors averaged over the period of 24–36 h of travel are in the ranges of 0.30–0.36, 0.23–0.30 and 0.19–0.21 for the 925-, 850- and 700-hPa particle trajectories, respectively.

The effectiveness of enhancing either temporal or spatial resolution of wind data for the improvement of trajectory accuracy is found to vary with the meteorological situation. When intervals of 12 h and 320 km are assumed to be the resolution of wind observations, enhancing the spatial resolution to a 160-km interval improves the accuracy more than enhancing the temporal resolution to a 6-h interval in case 1, in which the synoptic scale air flow pattern associated with the Siberian High changes slowly with time. On the other hand, the opposite is true in cases 2 and 3, although the difference in the improvements by the two different enhancements of resolution is small in case 2.

It is found that the estimated accuracy of a trajectory model and its sensitivity to the wind data density can vary significantly with the resolution of the reference wind data sets. According to the present results, the use of a data set with 1-h and 80-km intervals as the reference fields can result in a significant underestimation of transport errors and may exaggerate the effectiveness of enhancing the temporal density for the improvement of trajectory accuracy.

The present results indicate that the accuracy of an isobaric model is generally comparable to that of a 3D model, when data sets with 12-h and 320-km intervals are used. Under a strongly baroclinic condition, however, the isobaric model can give a very large trajectory error.

The fair agreement of the simulated reference fields with the observations supports the applicability of the present results to the real atmosphere. Additional cases would help to build up the confidence in the generality of the major results found in this study.

## 7. Acknowledgements

This study is supported by the Ministry of Environment and the Ministry of Science and Technology through the G7 project on Research and Development on Technology for Global Environmental Monitoring and Climate Change Prediction. Authors wish to thank Drs. Seung-Man Lee, In-Young Lee and Hye-Young Chun for their important remarks on this paper. They also wish to express their thanks to the two anonymous reviewers for their valuable suggestions which brought significant improvements in this paper. Thanks are also extended to Captain David Martens for the review of English.

## REFERENCES

Akima, H. 1970. A new method of interpolation and smooth curve fitting based on local procedures. *J. Assoc. Com. Mach.* **17**, 589–602.

Clarke, J. F., Clark, T. L., Ching, J. K. S., Haagenson, P. L., Husar, R. B. and Patterson, D. E. 1983. Assessment of model simulation of long-distance transport. *Atmos. Environ.* **17**, 2449–2462.

Doty, K. G. and Perkey, D. 1993. Sensitivity of trajectory calculations to the temporal frequency of wind data. *Mon. Wea. Rev.* **121**, 387–401.

Draxler, R. R. 1987. Sensitivity of a trajectory model to the spatial and temporal resolution of the meteorological data during CAPTEX. *J. Climate Appl. Meteor.* **26**, 1577–1588.

Ferber, G. L., Hefftner, J. L., Draxler, R. R., Lagomarsino, R. J., Thomas, F. L., Dietz, R. N. and Benkovitz, C. M. 1986. *Cross-Appalachian tracer experiment (CAPTEX '83).* Final Report, Environ. Res. Lab., Silver Spring, Md., Tech. Memo. ERL ARL-142, 60 pp.

Haagenson, P. L., Kuo, Y.-H., Skumanich, M. and Seaman, N. L. 1987. Tracer verification of trajectory models. *J. Climate Appl. Meteor.* **26**, 410–426.

Hoecker, W. H. 1977. Accuracy of various techniques for estimating boundary-layer trajectories. *J. Appl. Meteor.* **16**, 374–383.

Kahl, J. D. and Samson, P. J. 1986. Uncertainty in trajectory calculations due to low resolution meteorological data. *J. Climate Appl. Meteor.* **25**, 1816–1831.

Kuo, Y.-H., Skumanich, M., Haagenson, P. L. and Chang, J. S. 1985. The accuracy of trajectory models as revealed by the observing system simulation experiments. *Mon. Wea. Rev.* **113**, 1852–1867.

Pack, D. H., Ferber, G. J., Hefftner, J. L., Telegadas, K., Angell, J. K., Hoecker, W. H. and Machta, L. 1977. Meteorology of long-range transport. *Atmos. Environ.* **12**, 425–444.

Rolph, G. D. and Draxler, R. R. 1990. Sensitivity of three-dimensional trajectories to the spatial and temporal densities of the wind field. *J. Appl. Meteor.* **29**, 1043–1054.

Tremback, C. J. 1990. *Numerical simulation of a mesoscale convective complex: model development and numerical results.* Colorado State University, Department of Atmospheric Science, 465, 247 pp.

Tremback, C. J. and Kessler, R. 1985. *A surface temperature and moisture parameterization for use in mesoscale numerical models.* Preprints, 7th Conference on Numerical Weather Prediction. June 17–20, Montreal, Quebec, Canada, AMS.

Tremback, C. J., Tripoli, G. J. and Cotton, W. R. 1985. *A regional scale atmospheric numerical model including explicit moist physics and a hydrostatic time-split scheme.* Preprints, 7th Conference on Numerical Weather Prediction. June 17–20, Montreal, Quebec, Canada, AMS.

Tripoli, G. J. and Cotton, W. R. 1982. The Colorado State University three-dimensional cloud/mesoscale model. Part I: General theoretical framework and sensitivity experiments. *J. de Rech. Atmos.* **16**, 185–219.